EPJ Web of Conferences **89**, 01001 (2015)
DOI: 10.1051/epjconf/20158901001

The Innsbruck/ESO sky models and telluric correction tools*

The possibility of atmospheric monitoring for Čerenkov telescopes

S. Kimeswenger[1,2,a], W. Kausch[2,3], S. Noll[2], and A.M. Jones[2]

[1]Instituto de Astronomía, Universidad Católica del Norte, Avenida Angamos 0610, Antofagasta, Chile
[2]Institute for Astro- and Particle Physics, University of Innsbruck, Technikerstrasse 25/8, 6020 Innsbruck, Austria
[3]Department of Astrophysics, University of Vienna, Türkenschanzstrasse 17, 1180 Vienna, Austria

Abstract. Ground-based astronomical observations are influenced by scattering and absorption by molecules and aerosols in the Earth's atmosphere. They are additionally affected by background emission from scattered moonlight, zodiacal light, scattered starlight, the atmosphere, and the telescope. These influences vary with environmental parameters like temperature, humidity, and chemical composition. Nowadays, this is corrected during data processing, mainly using semi-empirical methods and calibration by known sources. Part of the Austrian ESO in-kind contribution was a new model of the sky background, which is more complete and comprehensive than previous models.

While the ground based astronomical observatories just have to correct for the line-of-sight integral of these effects, the Čerenkov telescopes use the atmosphere as the primary detector. The measured radiation originates at lower altitudes and does not pass through the entire atmosphere. Thus, a decent knowledge of the profile of the atmosphere at any time is required. The latter cannot be achieved by photometric measurements of stellar sources. We show here the capabilities of our sky background model and data reduction tools for ground-based optical/infrared telescopes. Furthermore, we discuss the feasibility of monitoring the atmosphere above any observing site, and thus, the possible application of the method for Čerenkov telescopes.

1. Introduction

Correcting the sky background is important for maximising the amount of data from a ground-based astronomical observation in the near ultraviolet (NUV), optical (VIS), and infrared (IR). Typically, it is corrected by using sky observations and/or known spectrophotmetric standard stars, called telluric standard stars. However, sometimes these observations are not available and additionally telescope time is operationally expensive. Also, predicting the effect of the sky background for a given observation allows for better exposure time estimates needed for scheduling the telescope time. As part of the entrance fee to the European Southern Observatory (ESO), Austrian universities developed software modules for various projects (so-called in-kind projects). At the University of Innsbruck[1], we created a comprehensive sky background model. It was originally for new exposure time calculators ([1]), and was thereafter extended. Two data reduction tools were also developed for correcting the sky emission lines by manipulating reference sky spectra (`skycorr`) [2] and atmospheric absorption features (`molecfit`) [3,4]. The latter is based on fitting an atmospheric radiative transfer model to the observed spectra. Previous work was done by [5,6], and references therein. Nevertheless, to our knowledge, this is the first freely available general purpose package, covering such a large wavelength range from 0.3 to 30 μm, tested with such a large number of different resolutions ($100 \leq R = \frac{\lambda}{\Delta\lambda} \leq 1\,000\,000$) and with photometric wide band data. Our models were investigated using data from the ESO archive, which span over nearly 15 years, along with meteorological input information from weather forecast and climate research centres, as well as in-situ probes. We present the sky background model and focus on a few topics that are relevant for Čerenkov telescopes. We furthermore conducted first tests on adapting the data reduction tools for other observing sites. Finally, we discuss the feasibility of using them for atmosphere monitoring and data reduction for high energy experiments.

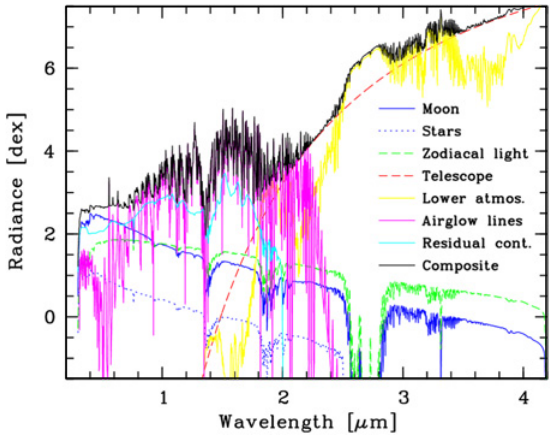

Figure 1. The Innsbruck/ESO sky model ([1]) for a half-moon phase and average humidity calculated for the VLT/Cerro Paranal. The black line shows the sum of the components (coloured lines, see figure legend).

* Based on ESO archival data and observations obtained in programme ID 491.L-0659 at ESO VLT.
[a] e-mail: `Stefan.Kimeswenger@gmail.com`; presenting author
[1] `http://www.uibk.ac.at/eso`

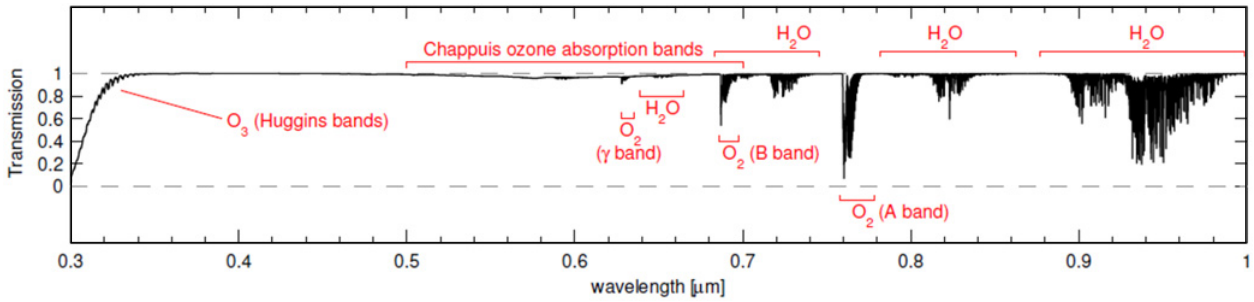

Figure 2. Absorption spectrum of the sky between 300 and 1000 nm calculated with LBLRTM (resolution $R = 10\,000$) for Cerro Paranal according to [1]. The main molecular contributions in this wavelength range are from O_2, H_2O, and O_3.

2. The model

We developed an atmospheric radiation model for the Very Large Telescope (VLT) of ESO at Cerro Paranal in the Atacama desert. It comprises all relevant components, i.e. thermal molecular radiation and absorption in the atmosphere, scattered starlight, zodiacal light, scattered moonlight, and non-thermal airglow line and continuum emission arising from chemiluminiscence in the mesopause and beyond (see Fig. 1). The model [1] covers the entire wavelength range from the NUV to the IR.

2.1 Thermal components of the atmosphere

The thermal components of the radiation and absorption in the atmosphere are computed with the help of the radiative transfer code Line-By-Line Radiative Transfer Model (hereafter LBLRTM, [7]). The internal resolution of LBLRTM is limited to $R \approx 4\,000\,000$, which is resampled to a user definable value in a subsequent step. LBLRTM requires as input a line database that contains information on molecular properties. At the time being, we use the `aer_v_3.2`, which is based on the High Resolution Transmission (HITRAN) 2008 data base [8] and is delivered in conjunction with the LBLRTM package. Imaging atmospheric Čerenkov telescopes observe light between the atmospheric ozone cutoff at 300 nm (O_3 Huggins bands) and the mid of the visual spectrum (depending on the used PMTs it can even be up to 700 nm) arising mainly at an altitude of 8 to 10 km [9]. Gamma rays at the low energy end of the observed spectrum may also produce showers at even higher altitudes, while very high energetic photons impact deeper into the atmosphere. Thus an integration over a large path is observed. The latter requires a profound understanding of all light scattering and absorption physics. This wavelength range is dominated by scattering, and the blue end is limited by ozone absorption (Huggins and Hartley bands) at ~300 nm. An overview of the molecular absorption in the UV/VIS regime is given in Fig. 2. The currently used line database `aer_v_3.2` is based on HITRAN 2008 which is limited to $\lambda \geq 400$ nm. The next update of the sky background model will be based on HITRAN 2012, which extends the available wavelength range towards the UV for O_3, H_2O, H_2, HF and HCl.

Another input for the radiative transfer code is an atmospheric profile. We use an atmospheric profile created by means of merging a standard atmosphere[2], on-site meteorological measurements[3], and the 3D Global Data Assimilation System (GDAS) model[4] (cf. [5]). The GDAS model provides a world-wide $1^\circ \times 1^\circ$ grid of atmospheric profiles containing the pressure, temperature, and the relative humidity as function of altitude. We interpolated the profiles of the four closest grid points (Fig. 3) to achieve a representative set of atmospheric profiles for Cerro Paranal. The GDAS data are available since 2005 and are calculated with a time sampling of 3^h. Thus, also a good time coverage is guaranteed. A temperature comparison of these profiles with the ground-based measurements of the on-site meteorological monitoring facilities resulted in good agreement ($\Delta T \sim 1°$C), while the modelled relative humidity is slightly higher in comparison with the measured ones. This is most probably the influence of the two GDAS grid points above the sea (see Fig. 3). The AUGER facility in Argentina ([10]) use a similar technique with better agreement, as this observing site is not as close to the sea.

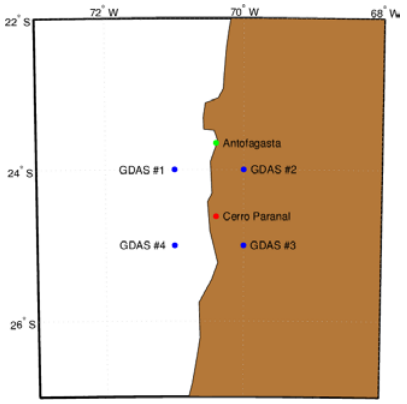

Figure 3. The GDAS model provides atmospheric profiles by a world-wide $1^\circ \times 1^\circ$ grid. For Cerro Paranal, we use a profile created by interpolating the closest four grid points (labelled GDAS #1 to #4). The results were compared and extensively tested with e.g. radiometer measurements [4]. A new access is the exact recalculation of the forecast by a nested grids down to a resolution of 1 km and using the complete ground topography around the site [15]. We plan to implement this soon.

[2] `http://www.atm.ox.ac.uk/RFM/atm/`
[3] `http://archive.eso.org/asm/ambient-server`
[4] `http://www.ready.noaa.gov/gdas1.php`

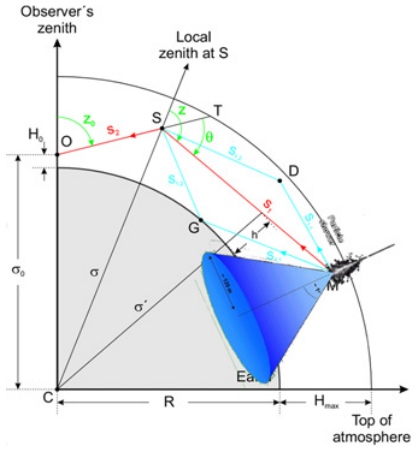

Figure 4. The 3D scattering model scheme as developed in [16] and with recently improved aerosol investigations of [17]. This can be applied also for a radiation propagation model from air showers.

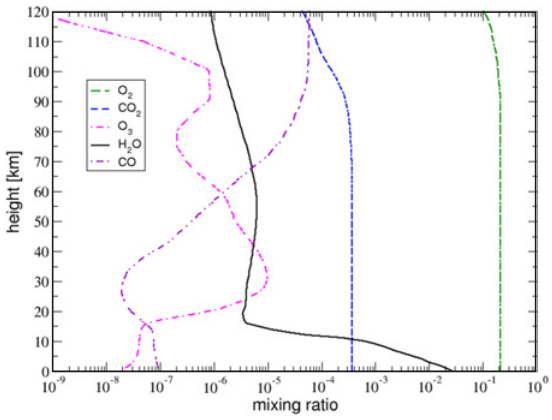

Figure 5. A typical profile of the height distribution of the volume mixing ratios of different prominent molecules.

2.2 Scattered light

Scattered light from extended sources (e.g. zodiacal light and airglow), is estimated by 3D single scattering calculations and a multiple scattering correction. Our model includes a detailed 3D code with double and multiple scattering approximations including ground reflection (Fig. 4).

We use the particle distribution from Rayleigh scattering as an approximation for the absorbing molecules. This is a good approach for molecules with constant abundance as function of height, e.g. O_2 (Fig. 5), and suitable for molecules with variable height abundances in the lower atmosphere. The corresponding airmass factor depends on the viewing geometry, the scattering properties of the atmosphere, and the vertical distribution of the absorber. Polynomial corrections, as typically derived and used in stellar photometry, take the curvature of the layers into account, but assume a normal exponential density scale with a scale height of about 8 km ([11, 12]). They can only be used for the Rayleigh scattering of O_2 and N_2 as used in [13] for Mauna Kea/Hawaii or by [14] for Cerro Paranal, and not for ozone, water vapour, and aerosols. Thus, a dedicated handling has to be performed for the other species (see [16] for more details). The correct airmass factor can be derived from integrations over the thin layer formula of van Rhijn.

2.3 Scattered Moonlight model

As shown in Fig. 1, the Moon is the brightest source of the sky background flux in NUV/VIS, when it is above the horizon. We have developed an advanced scattered moonlight model as part of the sky background model for ESO at Cerro Paranal ([16–18]). This model uses the solar spectrum as the initial input, a lunar albedo model, and 3D scattering calculations for the Moon as a point source. The scattering code includes scattering and absorption by molecules and particles. The scattered moonlight model was investigated and verified with ESO archive data [19] and data from a dedicated ESO VLT observing proposal. The scattered moonlight model is spectroscopic in the entire sky model range and is more physical and accurate than the previous, commonly used, photometric model based on V band data only [20].

2.4 Airglow

The intensity and variability of airglow emission (lines and continuum) is derived by a semi-empirical model based on more than 1000 high signal-to-noise spectra from Cerro Paranal by [19] taken between 04/1999-02/2005. The sky background model [1] can be used for site characterisation to estimate the sky brightness by incorporating averaged atmospheric data appropriate for the observing site. The thermal components calculated by LBLRTM, which dominate in the tropospheric region, are based on averaged atmospheric profiles. Creating a model for the non-thermal radiation in the upper atmosphere is complicated, as airglow varies on several time scales, from minutes (e.g. gravity waves) to decades (e.g. solar cycle). Figure 6 shows the variations found for Cerro Paranal, based on solar activity, seasonal (bi-monthly) variations, and the time during the night. The latter is a signature of the long lasting grazing illumination by the sun of the very high atmospheric layers, as well as the decline of the chemiluminescence processes during the cooling of the night. Moreover, periodic dynamical variations by e.g. thermal tides or global transport processes are important. Therefore, the Innsbruck/ESO sky model can be adapted to any observing site by averaging atmospheric profiles and adapting the airglow model. However, the latter is a non-trivial issue and requires some long-term monitoring. It might be important for threshold levels to separate spurious detection by sky background.

3. Accuracy

While the absorption by molecules like O_2 hardly vary with time and weather conditions, the H_2O content of the atmosphere is not easy to predict. The analysis of the GDAS profiles showed that the local microclimate dominates. Thus, a large data set using several years of

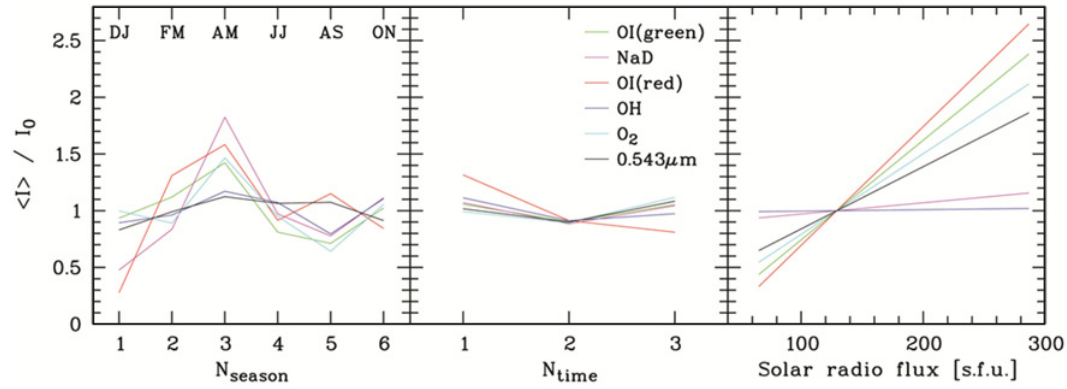

Figure 6. Averaged airglow model derived from the ESO data showing different line groups and their dependence on season (left panel: bimonthly averages starting with December+January = DJ), on the time within the night (middle panel: 1=early night, 2=middle, 3=late night), and solar radio flux measurements (right panel). This provides predictions for the sky background and background variability for each wavelength and thus input information for e.g. trigger thresholds.

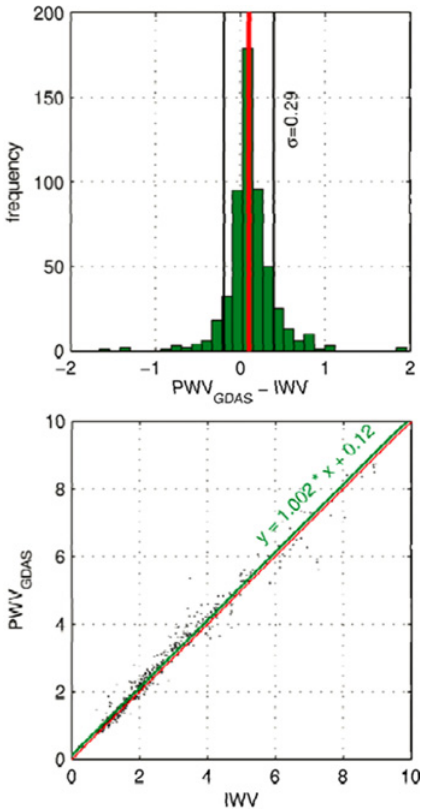

Figure 7. The PWV derived by spectral fitting compared to the IWV measured by HATPRO.

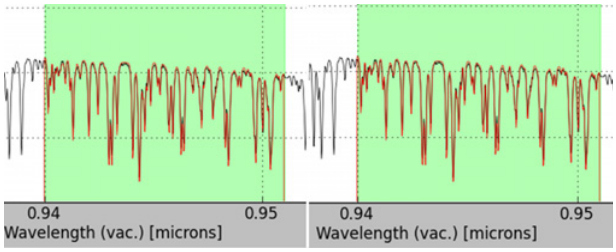

Figure 8. The H_2O lines fitted in the optical wavelength range (left) vs. the calculated ones using a PWV derived from fitting in the NIR (right). Even though the absolute values differ in this non-optimal case by about 0.25 mm (11%), the resulting modelled spectra look almost identical.

the VLT X-Shooter archive was reduced and investigated. This spectrograph was chosen, as it provides a spectrum from the NUV at 0.3 μm up to the near IR (NIR) at 2.5 μm simultaneously with a medium resolution of $3\,000 \leq R \leq 18\,000$. In the NIR, the absorption by water vapour ([4], Figs. 7, 8 and 9) and CO_2 as shown in [21] can be studied with high accuracy (Fig. 10).

During January, February, and August through December 2012, data from a microwave Humidity And Temperature PROfiling microwave radiometer (HATPRO, [22]) at Cerro Paranal were made available. We used 549 telluric standard star observations with X-Shooter in this period. The mean difference of the precipitable water vapour (PWV), as derived from the fitting of the astronomical spectra, and that of the integrated water vapor (IWV) measured by the HATPRO facility, was, as shown in Fig. 7, about 0.10 mm. As the correlation shows, this difference is mostly independent of the absolute value of the humidity. Moreover, the fitting was performed by means of GDAS profiles. Using HATRO-based atmospheric profiles did not improve the results ([4]). Therefore, our fitting is robust.

Some differences in the fitted PWV for the stronger NIR and VIS water vapour bands were found. This study is of special interest, as potential atmospheric monitoring facilities with smaller instruments can measure more easily in the VIS wavelength range than in the NIR (Figs. 8, 9).

The investigation of the aerosol scattering showed that the typical particle size distributions for remote continental aerosols ([23,24]) or scattering phase function parametrisations, as e.g. used in the widely spread model of [20], are not sufficient to describe our measurements. For that purpose spectra of empty sky fields at six different angular distances from the moon (7, 13, 20, 45, 90, and 110°) at three different moon phases were taken with X-Shooter (Fig. 11). Since especially the low angle forward scattering fit poorly, modified aerosol properties had to be applied ([17], Fig. 12).

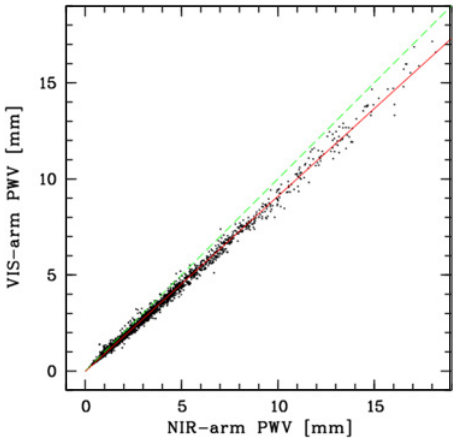

Figure 9. Comparison of the PWV in mm as derived from X-Shooter VIS-arm and NIR-arm spectra. The red solid line shows the result of a regression analysis. The green dashed line indicates the unity relation.

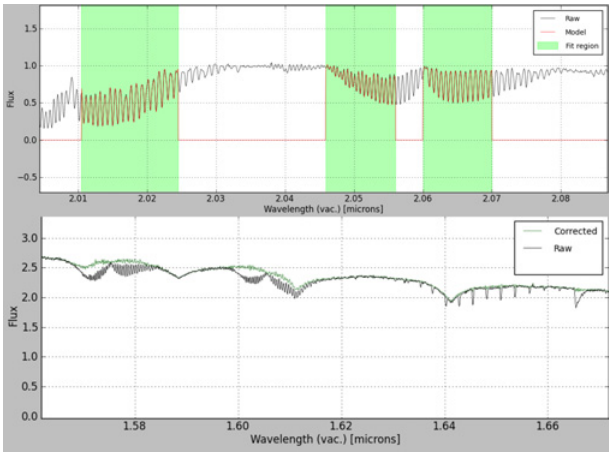

Figure 10. The CO_2 lines are fitted in the K band (upper panel). The resulting profile can be used to correct other spectral regions, where fitting might be influenced otherwise by lines of the targets (lower panel).

4. Adaption for atmospheric monitoring for Čerenkov telescopes

The airmass factor depends on the viewing geometry, the atmospheric scattering properties, and the vertical distribution of the absorber. The absorption as a function of the airmass will be different from the extinction by Rayleigh scattering caused by the smoothly (nearly) exponentially declining molecular absorbers like N_2 or O_2. As shown in Fig. 13, water vapour is strongly concentrated at lower altitudes. Most likely the same applies for aerosols, which are known to vary strongly with time and site (e.g. the Sahara dust for some seasons in Tenerife). Moreover, the peak of the ozone absorption at higher levels will cause a completely different behaviour. In particular, this is important for the use of an extinction curve derived by measurements of standard stars with photometers. They are unable to distinguish between the quasi continuum caused by the ozone Huggins and Chappuis bands and extinction by scattering (Fig. 14).

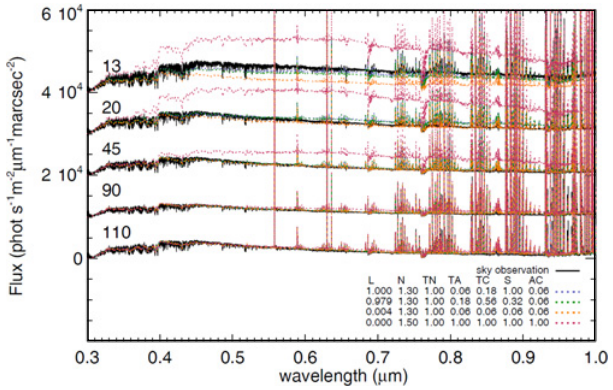

Figure 11. The observations of the scattered moonlight in the night 2013-07-23 (black lines). Various sky emission models with different aerosol properties are overlaid. The flux is given in photons s^{-1} m^{-2} μm^{-1} $arcsec^{-2}$ and shifted for clarity by 10^4 each (see [17]). A few aerosol mixes out of a large extensive grid of models is overlaid. Data in the table insert: L = Likelihood, N = optical refraction index, and the used fractions of the Tropical Nucleation (TC), Tropical Accumulation (TA) Tropical Coarse (TC), Stratospheric (S) and additional coarse mode (AC).

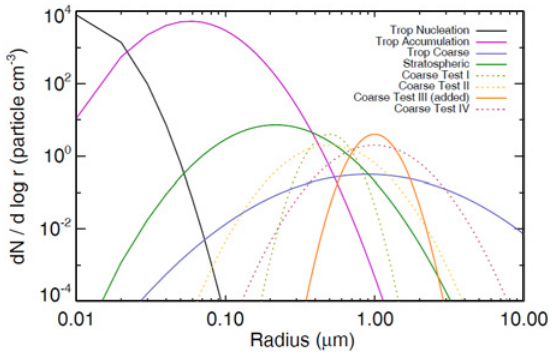

Figure 12. Standard aerosol size distributions (log normal) plus additional components required for deriving the appropriate optical properties.

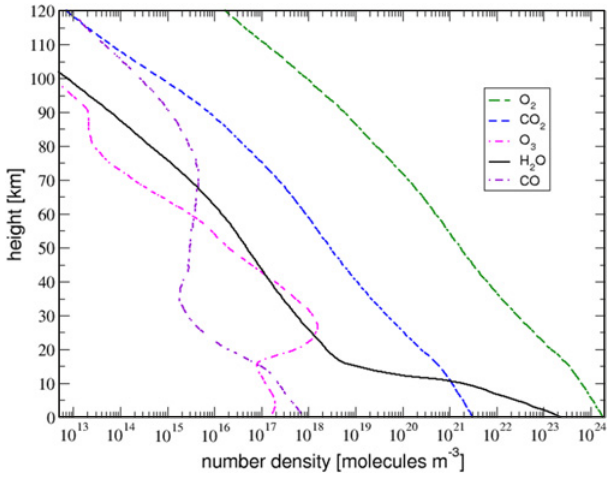

Figure 13. The vertical distribution of the most important molecules in absolute concentrations ($\propto$ effective absorption cross section). While H_2O is strongly concentrated in the ground layers and behaves only above 18 km proportional to the pressure gradient like O_2, ozone peaks between 20 and 35 km.

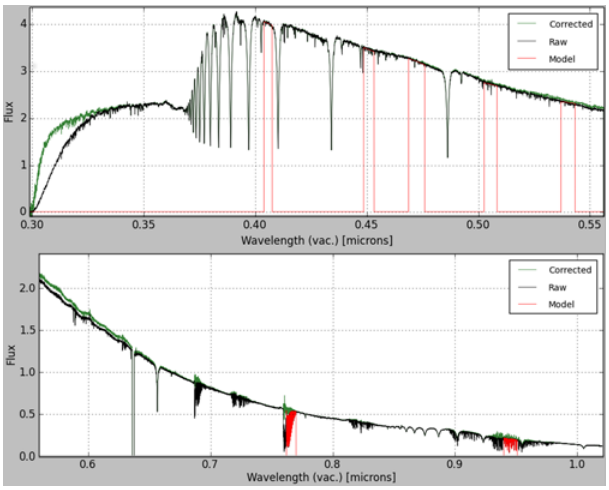

Figure 14. The effect of the quasi continuum by the ozone Huggins and Chappuis absorption bands shown on a ESO X-Shooter standard star spectrum corrected with `molecfit` (upper: UV arm, lower: VIS arm). Below 0.307 μm the star should have a nearly constant spectrum. The flux decrease in the corrected spectrum is caused by high inaccuracies due to the extremely low signal of the spectrum.

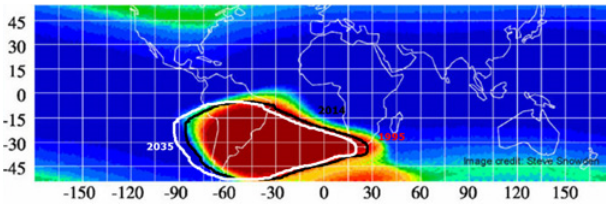

Figure 15. The movement of the SAA since the ROSAT measurements ([26]) for the typical lifetime of an astronomical facility like CTA.

However, the stratospheric ozone absorption is irrelevant for Čerenkov air showers, generated in the troposphere.

The variability of the solar activity and the geometry of the van Allen belt might influence the charged cosmic ray particles also generating showers producing Čerenkov light. While the solar flux is regularly monitored (see also Sect. 2.4), we have to expect changes due to the movement of the South Atlantic Anomaly (SAA) by about 0.3° per year. This originates from a differential rotation of the inner iron core against the crust of the earth ([25,26], Fig. 15). As it traps cosmic ray particles efficiently ([27]), changes will occur. This has to be taken into account over a typical construction and operation lifetime of an astronomical facility like the Čerenkov Telescope Array (CTA).

Finally, we carried out a test for this conference, using an extremely different observatory site. The purpose of this test was (a) to test the portability of our `molecfit` fitting procedure (see Sect. 1) to a humid low-altitude site with a frequent inversion layer and (b) to test it with a small facility more appropriate for atmospheric monitoring. The 60 cm telescope ([28,29], Fig. 16) of the observatory in Innsbruck was used. The data were taken on 2014-01-17 and the telescope was equipped with a small off-the-shelf echelle spectrograph (Fig. 17, [30]). This model is fairly wide spread at small facilities, and was already

Figure 16. The Observatory in Innsbruck, a valley with local pollution effects, humid weather conditions and a frequent inversion layer. This location is a testbed for conditions extremely different to those the codes were designed for.

Figure 17. The off-the-shelf echelle spectrograph eShel [30] as used for the tests at the Innsbruck 60 cm telescope (photo courtesy Oliver Thizy, `http://www.shelyak.com`).

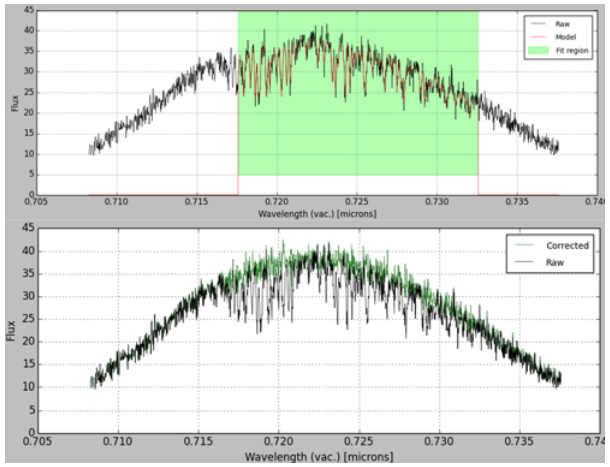

Figure 18. One single order of a 5 min echelle spectrum of a 4th magnitude star with the Innsbruck 60 cm telescope. The spectrum was neither flat-fielded nor corrected for instrumental response before applying `molecfit`.

used to obtain high-precision measurements ([31]). To test the feasibility for a meteorological monitoring on the fly without a dedicated data reduction, only the raw spectrum of one order was used (Fig. 18). The resulting PWV$= 39.8 \pm 2$ mm (about 20 times the typical value found at Cerro Paranal) was fairly close to the radiosonde measurement of 42 mm reported by the airport (about 1 km from the observatory).

5. Conclusions

Our atmospheric model based on a synthetic radiative transfer calculation of molecules and scattering processes can be supported easily by various measurements with small scale facilities. But while a simple photometric system on reference stars is unable to derive profile properties, a spectroscopic facility with a fairly small resolution of $R \approx 10\,000$ is sufficient to retrieve much better information. It is able to separate e.g. O_3 absorption from extinction by scattering processes. This is not possible with photometric observations of standard stars at robotic telescopes. As already shown by us in [1] and independently at the Pierre Auger facilities by [10], a properly adapted GDAS model already gives a very good description. This can be now further improved including the grid refinements down to 1 km resolution described by [15]. But moreover fitting by only a few spectral lines provides a nearly perfect profile and improves significantly this input of the GDAS profiles (interpolation in space $1^\circ \times 1^\circ$ and time 3^h). The major difference of our method to measurements with LIDARS is, that we have not to interpolate or extrapolate the aerosol properties assuming standard optical behaviour. H.E.S.S. uses two spectral points at 355 and 532 nm ([32]) to interpolate, while MAGIC uses one spectral point at 532 nm ([33]) to extrapolate. As we have shown [17,18] the wavelength dependency is strongly variable and moreover differs at least for the region in northern Chile completely from those in classical investigations given in geophysics literature mainly originating from locations dominated by particles produced by humans (see Fig. 11). Our strength is that we are able to obtain profile and optical properties at all the wavelengths where the instruments works. Moreover no generation of illumination sources, which may influence nearby other astronomical facilities are required by this purely passive measurement.

The scattering code, including ground reflectivity and multiple scattering, can certainly be also adopted for reconstructing the light/signal from Čerenkov showers.

Our tests with the Innsbruck 60 cm telescope ([28,29]) show that spectroscopy of sufficient quality can be achieved by 50–80 cm telescopes and an off-the-shelf echelle spectrograph ([30,31]).

This project made use of the ESO archive facility. This study was carried out in the framework of the Austrian ESO In-Kind project funded by Austrian Ministry of Science (BM:wf) under contracts BMWF-10.490/0009-II/10/2009 and BMWF-10.490/0008-II/3/2011, and by the project IS538003 (Hochschulraumstrukturmittel). This publication is also supported by the Austrian Science Fund (FWF) project P26130.

References

[1] S. Noll, W. Kausch, M. Barden, A.M. Jones, C. Szyszka, S. Kimeswenger, J. Vinther, Astronomy and Astrophysics, **543**, A92 (2012)

[2] S. Noll, W. Kausch, S. Kimeswenger, M. Barden, A.M. Jones, A. Modigliani, C. Szyszka, J. Taylor, Astronomy and Astrophysics, **567**, A25 (2014)

[3] A. Smette, H. Sana, S. Noll, H. Horst, W. Kausch, S. Kimeswenger, M. Barden, C. Szyszka, A.M. Jones, A. Gallene, J. Vinther, P. Ballester, Astronomy and Astrophysics, in press, [arXiv:1501.07239] (2015)

[4] W. Kausch, S. Noll, A. Smette, S. Kimeswenger, M. Barden, C. Szyszka, A.M. Jones, H. Sana, H. Horst, F. Kerber, Astronomy and Astrophysics, in press, [arXiv:1501.07265] (2015)

[5] A. Seifahrt, H.U. Käufl, G. Zängl, J.L. Bean, M.J. Richter, R. Siebenmorgen, Astronomy and Astrophysics, **524**, A11 (2010)

[6] G. Lombardi, E. Mason, C. Lidman, A.O. Jaunsen, A. Smette, Astronomy and Astrophysics, **528**, A43 (2011)

[7] S.A. Clough, M.W. Shephard, E.J. Mlawer, J.S. Delamere, M.J. Iacono, K. Cady-Pereira, S. Boukabara, P.D. Brown, Journal of Quantitative Spectroscopy and Radiative Transfer, **91**, 233 (2005)

[8] L.S. Rothman, I.E. Gordon, A. Barbe, D.C. Benner, P.F. Bernath, M. Birk, V. Boudon, L.R. Brown, A. Campargue, J.-P. Champion, K. Chance, L.H. Coudert, V. Dana, V.M. Devi, S. Fally, J.-M. Flaud, R.R. Gamache, A. Goldman, D. Jacquemart, I. Kleiner, N. Lacome, W.J. Lafferty, J.-Y. Mandin, S.T. Massie, S.N. Mikhailenko, C.E. Miller, N. Moazzen-Ahmadi, O.V. Naumenko, A.V. Nikitin, J. Orphal, V.I. Perevalov, A. Perrin, A. Predoi-Cross, C.P. Rinsland, M. Rotger, M. Šimečková, M.A.H. Smith, K. Sung, S.A. Tashkun, J. Tennyson, R.A. Toth, A.C. Vandaele, J. Vander Auwera, Journal of Quantitative Spectroscopy and Radiative Transfer, **110**, 533 (2009)

[9] P.F. Grieder, *Extensive Air Showers: High Energy Phenomena and Astrophysical Aspects – A Tutorial, Reference Manual and Data Book* (Springer, Berlin Heidelberg), 1118p (2010)

[10] The Pierre Auger Collaboration, P. Abreu, M. Aglietta, M. Ahlers, et al., Astroparticle Physics **35**, 591 (2012)

[11] R.H. Hardie, *"Photoelectric Reductions", Chapter 8 of Astronomical Techniques, W.A. Hiltner (Ed), Stars and Stellar Systems, II* (University of Chicago Press, Chicago) pp. 178–208 (1962)

[12] A.T. Young, W.M. Irvine, Astronomical Journal, **72**, 945 (1967)

[13] C. Buton, Y. Copin, G. Aldering, P. Antilogus, C. Aragon, S. Bailey, C. Baltay, S. Bongard, A. Canto, F. Cellier-Holzem, M. Childress, N. Chotard, H.K. Fakhouri, E. Gangler, J. Guy, E.Y. Hsiao, M. Kerschhaggl, M. Kowalski, S. Loken, P. Nugent, K. Paech, R. Pain, E. Pácontal, R. Pereira, S. Perlmutter, D. Rabinowitz, M. Rigault, K. Runge, R. Scalzo, G. Smadja, C. Tao, R.C. Thomas, B.A. Weaver, C. Wu, Astronomy and Astrophysics, **549**, A8 (2013)

[14] F. Patat, S. Moehler, K. O'Brien, E. Pompei, T. Bensby, G. Carraro, A. de Ugarte Postigo, A. Fox, I. Gavignaud, G. James, H. Korhonen, C. Ledoux, S. Randall, H. Sana, J. Smoker, S. Stefl, T. Szeifert, Astronomy and Astrophysics, **527**, A91 (2011)

[15] J.C. Marin, D. Pozo, M. Curé, Astronomy and Astrophysics, **573**, A41 (2015)
[16] A.M. Jones, S. Noll, W. Kausch, C. Szyszka, S. Kimeswenger, Astronomy and Astrophysics, **560**, A91 (2013)
[17] A.M. Jones, S. Noll, W. Kausch, C. Szyszka, S. Kimeswenger, Astronomy and Astrophysics, submitted (2015)
[18] A.M. Jones, S. Noll, W. Kausch, C. Szyszka, S. Kimeswenger, The Messenger, **256**, 31 (2014)
[19] F. Patat, Astronomy and Astrophysics, **481**, 575 (2008)
[20] K. Krisciunas, B.E. Schaefer, Publications of the Astronomical Society of the Pacific, **103**, 1033 (1991)
[21] W. Kausch, S. Noll, C. Szyszka, A.M. Jones, A. Smette, S. Kimeswenger, M. Barden, H. Sana, H. Horst, EGU General Assembly Conference Abstracts, **15**, 7425 (2013)
[22] T. Rose, S. Crewell, U. Löhnert, C. Simmer, Atmospheric Research, **75**, 183 (2005)
[23] P. Warneck, J. Williams, 2012, *The Atmospheric Chemist's Companion* (Springer, New York), 438p (2012)
[24] C.F. Bohren, D.R. Huffman, *Absorption and scattering of light by small particles* (Wiley, New York), 544p (1983)
[25] E.G. Stassinopoulos, C.A. Staffer, *Forty-Year Drift and Change of the SAA* (NASA Goddard Spaceflight Center, Goddard) (2007)
[26] S.L. Snowden, *South Atlantic Anomaly Detector (SAAD) aboard ROSAT*, (NASA, Goddard Spaceflight Center, Goddard) (2002)
[27] O. Adriani, G.C. Barbarino, G.A. Bazilevskaya, et al., The Astrophysical Journal Letters, **737**, L29 (2011)
[28] S. Kimeswenger, Astronomische Gesellschaft Meeting Abstracts, **18**, 251 (2001)
[29] S. Kimeswenger, C. Lederle, S. Schmeja, B. Armsdorfer, Monthly Notices of the Royal Astronomical Society, **336**, L43 (2002)
[30] O. Thizy, F. Cochard, IAU Symposium, **272**, 282 (2011)
[31] S.K. Kozłowski, M. Konacki, M. Ratajczak, P. Sybilski, R.K. Pawłaszek, K.G. Hełminiak, Monthly Notices of the Royal Astronomical Society, **443**, 158 (2014)
[32] M. Bourgeat, M. Compin, S. Rivoire, G. Vasileiadis, AtmoHEAD'13 Workshop, Saclay, [arXiv:1311.3760] (2013)
[33] C. Fruck, M. Gaug, R. Zanin, D. Dorner, D. Garrido, R. Mirzoyan, L. Font, for the MAGIC Collaboration, ICRC 2013, Rio de Janeiro, [arXiv:1403.3591] (2014)